Appl. Phys. B (2017) 123:107
DOI 10.1007/s00340-017-6691-1

Applied Physics B
Lasers and Optics

Controlling optical beam shifts upon reflection from a magneto-electric liquid-crystal-based system for applications to chemical vapor sensing

Yuliya S. Dadoenkova[1,2,3] · Florian F. L. Bentivegna[4] · Viacheslav V. Svetukhin[2,5] · Andrey V. Zhukov[2,5] · Roman V. Petrov[1] · Mirza I. Bichurin[1]

Received: 16 November 2016 / Accepted: 28 February 2017 / Published online: 22 March 2017

Abstract We investigate the tunability of the Goos–Hänchen shift experienced by a Gaussian light beam reflected from a multilayered heterostructure consisting of a nematic liquid-crystal cell sandwiched between electrodes and deposited on a magneto-electric/non-magnetic bilayer. Our calculations account for the optical anisotropy of the magnetic layer and of the liquid-crystal cell, as well as for the inhomogeneous refractive index distribution in the latter due to the reorientation of its molecules. We show that the Goos–Hänchen shift can be enhanced and controlled via the voltage applied to the liquid crystal cell and the magnetization direction of the magnetic film. We propose to exploit the voltage-induced tunability of the Goos–Hänchen shift in this system to design an optical sensor devoted to the detection of chemical vapors in the vicinity of the structure.

✉ Yuliya S. Dadoenkova
yulidad@gmail.com

Florian F. L. Bentivegna
fb@enib.fr

Viacheslav V. Svetukhin
slava@sv.uven.ru

Andrey V. Zhukov
zhukovandreyv@mail.ru

Roman V. Petrov
initra@ya.ru

Mirza I. Bichurin
mirza.bichurin@novsu.ru

[1] Novgorod State University, Veliky Novgorod 173003, Russian Federation

[2] Ulyanovsk State University, Ulyanovsk 432017, Russian Federation

[3] Donetsk Institute for Physics and Technology, Donetsk 83114, Ukraine

[4] Lab-STICC (UMR 6285), CNRS, UBL, ENIB, 29238 Brest Cedex 3, France

[5] Institute of Nanotechnologies of Microelectronics of the Russian Academy of Sciences, Moscow 119991, Russian Federation

1 Introduction

The Goos–Hänchen effect is the longitudinal shift, in the incidence plane, of a reflected light beam with respect to the prediction of geometric optics [1, 2]. This Goos–Hänchen shift (GHS) can be attributed to the angular dispersion of the phase delay upon reflection at any surface or interface of a linearly polarized light beam [3]. Although this effect has been known for many decades, it still attracts considerable attention. During the last decade, numerous theoretical and experimental works have been devoted to the GHS, either in the conditions of total internal reflection or in the case of partial reflection and transmission [4]. Among its many proposed practical applications, the GHS has been suggested for instance for the design of chemical sensors [5, 6], biosensors [7], detectors, or detectors of surface roughness [8]. For all these applications, and for any additional ones, it is obviously important to be able to control and enhance the beam shifts. For that purpose, using functional materials, i.e., materials whose properties can be modified by an external source, can be of great interest.

To mention a few recent examples, the thermal control of the GHS in a prism-waveguide coupling system has been investigated [9]; the control of the GHS with a magnetic field has been demonstrated in magnetic materials [10, 11], including ferrofluids [12]; its control with external electric and magnetic fields in an electro-optic and magneto-electric

(ME) heterostructure has been investigated theoretically in [13, 14], where the linear ME interaction has been shown to lead to an increase of the longitudinal shift even in the absence of any applied electric field; the use of the GHS in an array of quantum dots has been proposed to obtain a 1×3 de/multiplexer with a 2-nm channel spacing [15]; similarly, exploiting the GHS for an electrically controlled one-to-three optical switch has been discussed in [16].

A class of materials whose optical properties can be externally controlled are liquid crystals (LCs) [17–20]. In [19, 20], for instance, the tuning of the GHS is studied theoretically for a light beam coupled through a ZnSe prism in an electro-optically tunable liquid-crystal layer in the Kretschmann–Raether geometry. However, as often, only effective refractive indices of the anisotropic LC layer are considered and the non-uniformity of their distribution due to the anchoring of the LC molecules at the cell boundaries is not taken into account.

In this paper, we investigate the control of the GHS experienced by a light beam reflected from a multilayered heterostructure consisting of an LC cell sandwiched between conducting electrodes and deposited on top of a ME/non-magnetic bilayer. Our calculations account for the optical anisotropy of the magnetic layer and of the LC cell, as well as for the non-uniform refractive index distribution in the latter. Finally, we propose to exploit the voltage-induced tunability of the GHS in this system, and its sensitivity to variations of the permittivity of the medium from which the optical beam is coming, in order to design an optical sensor devoted to the detection of chemical vapors in the vicinity of the structure.

2 Description of the system

Let us consider the reflection of an electromagnetic wave from a multilayered system consisting of a nematic liquid-crystal (LC) cell (thickness d_{LC}) surrounded by two indium-tin oxide (ITO) electrodes (thickness d_{ITO}) and deposited on a ME structure. The latter is made up of a magnetic yttrium–iron garnet (YIG) film (thickness d_{YIG}) epitaxially grown on a semi-infinite dielectric substrate of gadolinium–gallium garnet (GGG). The interfaces between the materials are parallel to the (xy) plane of a Cartesian system of coordinates. An electromagnetic wave of near-infrared wavelength λ_0, coming from the surrounding vacuum, impinges under oblique incidence angle θ the upper surface of the system. Without loss of generality, the plane of incidence can be chosen as (xz) and the incident (i) and reflected (r) waves can be decomposed into s- and p-components $E_{s,p}^{(i,r)}$ of their electric field strengths with respect to that plane. In the following, the time dependence of the optical fields is taken as $\exp(-i\omega t)$.

As a rule, when a monochromatic Gaussian wavepacket of elliptical polarization impinges on the uppermost surface of an optical structure, its reflection undergoes a non-negligible longitudinal GHS ΔL in the plane of incidence (in our case, along the x-axis), as shown in Fig. 1.

In the system under consideration, a voltage can be applied to the ITO electrodes to modify the LC refractive index through a collective reorientation of its molecules. We assume the lateral dimensions of the cell (along the x and y directions) to be much larger than its thickness d_{LC}, so that side effects in the molecular alignment at the lateral boundaries of the cell can be neglected.

The anisotropic magnetic YIG slab is magnetized at saturation in the polar magneto-optical configuration, i.e., along the z-axis, and its magnetization can be reversed via an externally applied magnetic field. Thin epitaxial iron garnet films can be the seat of a linear ME coupling that is otherwise forbidden in bulk cubic crystals with a spatial inversion in their magnetic symmetry group [21]. The strength of that coupling, however, can greatly vary, depending on the film thickness, the crystal orientation

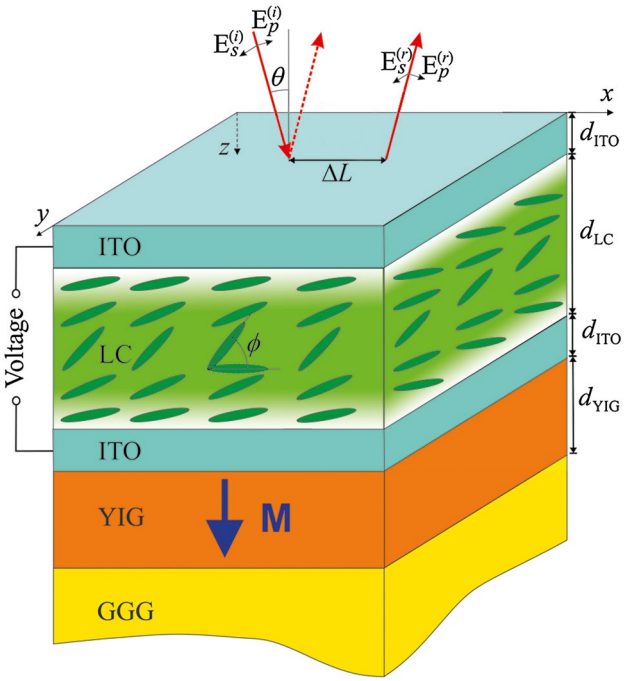

Fig. 1 Schematic of the structure ITO/LC/ITO/YIG/GGG: liquid-crystal (LC) cell (thickness d_{LC}) between indium-tin oxide (ITO) electrodes (thickness d_{ITO}) on an yttrium–iron garnet (YIG) film (thickness d_{YIG}) epitaxially grown on a semi-infinite dielectric substrate of gadolinium–gallium garnet (GGG). The saturation magnetization $\mathbf{M}=\{0, 0, M_s\}$ in the magnetic slab is perpendicular to the surfaces of the slabs. The s- and p-components of the incident (i) and reflected (r) optical electric fields are denoted $E_{s,p}^{(i,r)}$. The incidence angle is θ, and ϕ is the tilt angle of LC molecules. The longitudinal GHS is ΔL

of the film, and the presence of impurities, as well as on the value and direction of applied electric and magnetic fields. In Sect. 3, we will consider two extreme cases: with a negligibly small ME coupling and with the strongest coupling reported so far in the literature.

In the near-infrared domain, all materials except ITO can be considered transparent. The GGG dielectric substrate is homogeneous and isotropic, as are the ITO electrodes, and their relative dielectric permittivities are scalar and, respectively, denoted $\varepsilon^{(\mathrm{GGG})}$ and $\tilde{\varepsilon}^{(\mathrm{ITO})} = \varepsilon^{(\mathrm{ITO})} + i\eta^{(\mathrm{ITO})}$ ($\eta^{(\mathrm{ITO})} > 0$).

2.1 Permittivity of the liquid crystal

The cell contains a homogeneously aligned nematic LC consisting of uniaxial rod-shaped cyano-4′-pentylbiphenyl (or 5CB) molecules whose principal relative permittivities are denoted ε_1 and $\varepsilon_2 = \varepsilon_3$. We assume the collective alignment of the molecules to be parallel to the (xz) plane and characterized by a tilt angle ϕ with respect to the x-axis (Fig. 1). The constitutive material equations expressing the relationship of the electric displacement vector **D** and the magnetic induction **B** in the LC cell with the electric field **E** and the magnetic field **H** of the electromagnetic wave read:

$$D_i^{(\mathrm{LC})} = \varepsilon_0 \varepsilon_{ij}^{(\mathrm{LC})} E_j^{(\mathrm{LC})}, \quad B_i^{(\mathrm{LC})} = \mu_0 H_j^{(\mathrm{LC})}, \quad (i,j) = (x, y, z), \tag{1}$$

where ε_0 and μ_0 are the vacuum permittivity and permeability, and $\varepsilon_{ij}^{(\mathrm{LC})}$ are the relative permittivity tensor elements of the LC, only five of which take non-zero values given by:

$$\begin{aligned}
\varepsilon_{xx}^{(\mathrm{LC})} &= \varepsilon_1 \cos^2\phi + \varepsilon_3 \sin^2\phi, \\
\varepsilon_{yy}^{(\mathrm{LC})} &= \varepsilon_2 = \varepsilon_1, \\
\varepsilon_{zz}^{(\mathrm{LC})} &= \varepsilon_1 \sin^2\phi + \varepsilon_3 \cos^2\phi, \\
\varepsilon_{xz}^{(\mathrm{LC})} &= \varepsilon_{zx}^{(\mathrm{LC})} = \left(\varepsilon_3 - \varepsilon_1\right) \cos\phi \sin\phi.
\end{aligned} \tag{2}$$

When the voltage applied to the ITO electrodes exceeds a certain threshold value V_{th}, molecules rotate in the (xz) plane, but their rotation is not uniform within the LC cell due to their anchoring at each LC/ITO interface. In the limiting case of a uniform and infinitely strong orientational interaction of the LC molecules with the surfaces of the cell (so-called infinite anchoring [17]), Abdulhalim and Menashe have derived analytical expressions that describe with a good approximation the dependence of the tilt angle ϕ on the reduced z-coordinate $Z_{\mathrm{r}} = (z - d_{\mathrm{LC}})/d_{\mathrm{LC}}$, $0 \le Z_{\mathrm{r}} \le 1$ in the LC cell and on the applied voltage V [22]. Important parameters in these expressions are the pretilt angle ϕ_0 at zero voltage imposed by the anchoring of the molecules at the upper and lower cell boundaries (ϕ_0 is close to zero if the anchoring is strong), and the tilt angle ϕ_{c} at the center of the cell ($Z_{\mathrm{r}} = 1/2$) which, in the case of a strong anchoring, can be approximated as follows [23]:

$$\phi_{\mathrm{c}}(V) = \phi_0 + \left(\frac{\pi}{2} - \phi_0\right)\sqrt{1 - \left(\frac{V_{\mathrm{th}}}{V}\right)^2}. \tag{3}$$

Figure 2 shows the variation of the tilt angle ϕ in the LC cell with the applied voltage for a quasi-infinite anchoring, in which case ϕ is close to ϕ_{c} in a large fraction of the cell.

2.2 Permittivity and permeability of the magneto-electric film

Taking into account the linear ME interaction, the constitutive material equations in the magnetic YIG are [24]:

$$\begin{aligned}
D_i^{(\mathrm{YIG})} &= \varepsilon_0 \varepsilon_{ij}^{(\mathrm{YIG})} E_j^{(\mathrm{YIG})} + \alpha_{ij} H_j^{(\mathrm{YIG})}, \\
B_i^{(\mathrm{YIG})} &= \mu_0 \mu_{ij}^{(\mathrm{YIG})} H_j^{(\mathrm{YIG})} + \alpha_{ij} E_j^{(\mathrm{YIG})},
\end{aligned} \tag{4}$$

where $\varepsilon_{ij}^{(\mathrm{YIG})}$ and $\mu_{ij}^{(\mathrm{YIG})}$ are the relative permittivity and permeability tensor elements of YIG, and α_{ij} are the elements of its ME tensor. The latter is diagonal in crystals with cubic symmetry ($\alpha_{ij} = \alpha^{(\mathrm{YIG})}\delta_{ij}$, where δ_{ij} is the Kronecker delta).

It is well known that YIG exhibits good transparency properties in the near-infrared regime and is also magnetically bigyrotropic in that regime, i.e., its permittivity and permeability tensors both depend on the local magnetization. In the linear approximation, in the polar magneto-optical configuration and in crystals with cubic symmetry, they write [25]:

$$\begin{aligned}
\varepsilon_{ij}^{(\mathrm{YIG})} &= \begin{pmatrix} \tilde{\varepsilon} & if^{(e)}m_z & 0 \\ -if^{(e)}m_z & \tilde{\varepsilon} & 0 \\ 0 & 0 & \tilde{\varepsilon} \end{pmatrix}, \\
\mu_{ij}^{(\mathrm{YIG})} &= \begin{pmatrix} \tilde{\mu} & if^{(m)}m_z & 0 \\ -if^{(m)}m_z & \tilde{\mu} & 0 \\ 0 & 0 & \tilde{\mu} \end{pmatrix},
\end{aligned} \tag{5}$$

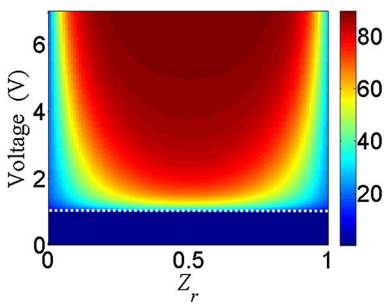

Fig. 2 Distribution of the tilt angle ϕ over the LC cell as a function of the applied voltage. The threshold voltage is $V_{\mathrm{th}} = 1$ V (*dotted line*), and the pretilt angle is $\phi_0 = 0.01°$

where $m_z = M_z/|\mathbf{M}|$, $\tilde{\varepsilon}$, and $\tilde{\mu}$ are the crystallographic components of the diagonal relative permittivity and permeability tensors, and $f^{(e,\,m)}$ are the linear gyroelectric and gyromagnetic coefficients of the crystal.

2.3 Goos–Hänchen shift

The GHS is deduced from the angular dispersion of the complex reflectivity of the structure. Due to the crystalline asymmetry of the LC cell and the anisotropy imposed in the YIG layer by the polar magnetization and the ME interaction, this reflectivity strongly depends on the state of polarization of the incoming and reflected beams. A reflection matrix connects the amplitudes of the p- and s-components of the reflected field to those of the incident field. It is derived using the well-known transfer matrix formalism [26], which involves solving the set of boundary conditions at each interface in the system:

$$E_j^{(a)}\Big|_{z=z_a^-} = E_j^{(b)}\Big|_{z=z_a^+},\quad H_j^{(a)}\Big|_{z=z_a^-} = H_j^{(b)}\Big|_{z=z_a^+}, \tag{6}$$

where $j = (x, y)$ and a and b $(a \neq b)$ denote adjacent media (successively, air, ITO, LC, ITO, YIG, and GGG) in the system, and $z_a = 0$, d_{ITO}, $d_{\mathrm{ITO}} + d_{\mathrm{LC}}$, $2d_{\mathrm{ITO}} + d_{\mathrm{LC}}$, $2d_{\mathrm{ITO}} + d_{\mathrm{LC}}$ $+\mathrm{d}_{\mathrm{YIG}}$ denote the successive positions of their common interfaces.

The reflection matrix has in general four non-zero complex components:

$$\begin{pmatrix} E_p^{(r)} \\ E_s^{(r)} \end{pmatrix} = \begin{pmatrix} R_{pp} & R_{ps} \\ R_{sp} & R_{ss} \end{pmatrix} \begin{pmatrix} E_p^{(i)} \\ E_s^{(i)} \end{pmatrix}. \tag{7}$$

Due to the symmetry of the YIG crystal, the pure imaginary off-diagonal components of the matrix verify $R_{ps} = R_{sp}$.

In the multilayered system, the reflections of the various angular components of the finite-sized incident Gaussian beam interfere along a line transverse to the average propagation direction of that beam. This leads to an angular dispersion of the phase shift of the electromagnetic field upon reflection, which results in an angular dispersion of both the amplitude and the phase of the reflection coefficients of the structure, from which the Goos–Hänchen shift can be derived. Specifically, the amplitude ΔL of the longitudinal GHS can be obtained with the stationary-phase approach [2]. Assuming a monochromatic incident Gaussian beam of waist w_0, the longitudinal shift of the reflected wavepacket can then be expressed as a GHS matrix whose elements are written as follows [27]:

$$\Delta L_{lm} = -\frac{\partial \psi_{lm}}{\partial k_x} + \frac{\partial \ln\left(|R_{lm}|\right)}{\partial k_x}\,\frac{\partial^2 \psi_{lm}}{\partial k_x^2}\left(w_0^2 + \frac{\partial^2 \ln\left(|R_{lm}|\right)}{\partial k_x^2}\right)^{-1}, \tag{8}$$

where $\psi_{lm}(k_x) = \arg\left[R_{lm}(k_x)\right]$, $\{l, m\} \in \{s, p\}$, are the phases of the four complex reflection coefficients for any given k_x component of the incident wavevector $\boldsymbol{k}$ along the x-axis. In view of sizing the amplitude of the GHS, it is convenient to introduce reduced GHS matrix elements as $\Delta X_{lm} = \Delta L_{lm}/\lambda_0$. It must be noted, however, that the shift that can be experimentally measured depends on the polarization states of both the incoming and reflected beams. The different components of that shift can be obtained using a polarizer and an analyzer before and after reflection, respectively.

3 Numerical results

In this section, we present the result of numerical calculations of the reflection coefficients and longitudinal shift for a Gaussian pulse (waist $w_0 = 50$ μm). The material parameters of all the constituents of the system are collected in Table 1. The value of the ME constant denoted $\alpha^{(\mathrm{YIG})}$ is the largest reported for a thin YIG film [21, 28]. Unless otherwise specified, the magnetization in the YIG layer points toward positive values of the z-axis.

3.1 Reflection coefficients

Figure 3 shows how the modulus of the diagonal component R_{pp} (Fig. 3a) of the reflection matrix, as well as that of the off-diagonal component $R_{sp} = R_{ps}$ (Fig. 3b, c), vary as functions of the incidence angle θ of the light beam and of the dc voltage applied to the LC cell. The complex profiles of the reflection coefficients result from a combination of interferences between the various waves propagating back and forth between the surface and interfaces of the system, on one hand, and of additional anisotropies due to the molecular alignment in the LC layer and the ME coupling in the magnetic layer, on the other. The interference pattern essentially varies with θ, while the anisotropies depend on the applied voltage and the value of the ME constant.

Table 1 Physical data used for calculations

Material	Thickness (μm)	Material parameters (at $\lambda_0 = 1$ μm)
ITO	$d_{\mathrm{ITO}} = 0.05$	$\varepsilon^{(\mathrm{ITO})} = 1.7057$, $\eta^{(\mathrm{ITO})} = 0.0337$ [29]
LC (5CB)	$d_{\mathrm{LC}} = 2.2$	$\varepsilon_1 = 15.7$, $\varepsilon_2 = \varepsilon_3 = 7.5$ [18]; $\phi_0 = 0.01°$
YIG	$d_{\mathrm{YIG}} = 2$	$\tilde{\varepsilon} = 5.0491$ [30], $\alpha = \alpha^{(\mathrm{YIG})} = 30$ ps/m [21] $f^{(e)} = -2.47\cdot10^{-4}$, $f^{(m)} = 8.76\cdot10^{-5}$ [31]
GGG	Semi-infinite	$\varepsilon^{(\mathrm{GGG})} = 3.7636$ [31]

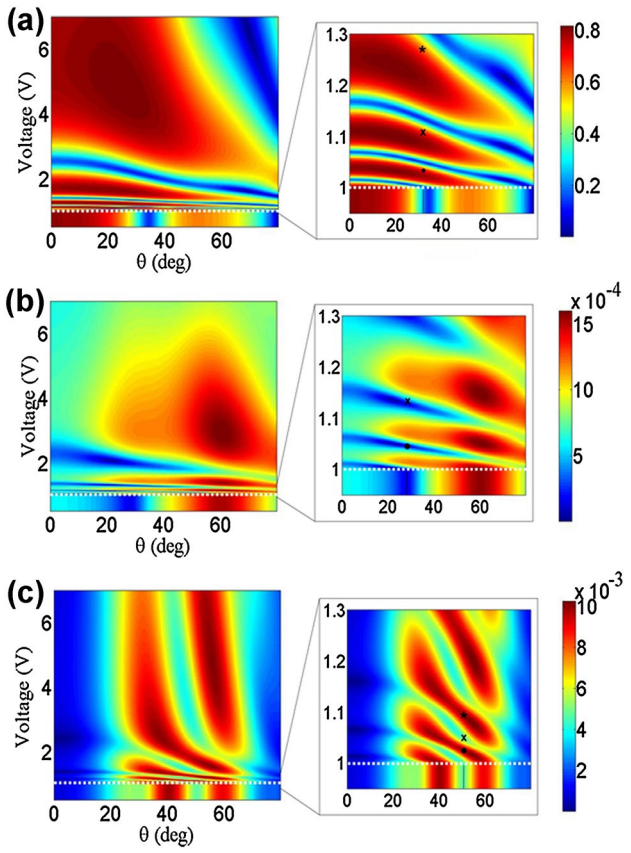

Fig. 3 Evolution of the modulus of the reflection coefficients with incidence angle θ and applied voltage: **a** $|R_{pp}|$ for any value of the ME constant α; **b** $|R_{ps}|$ for $\alpha=0$; **c** $|R_{ps}|$ for $\alpha=\alpha^{(\mathrm{YIG})}$. Insets show the corresponding reflection coefficients for near-threshold values of the applied voltage. The *white dotted lines* denote the threshold voltage $V_{\mathrm{th}}=1$ V. *Symbols* (•, ×, *) denote points of comparison between reflection coefficients in this figure and GHS in Fig. 5 (see Subsection 3.2)

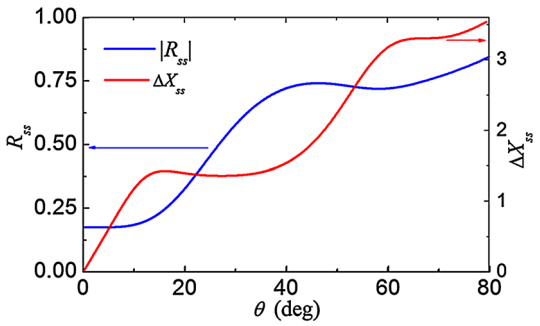

Fig. 4 Modulus $|R_{ss}|$ (*solid blue line*) and GHS ΔX_{ss} (*dashed red line*) as functions of the incidence angle θ for any value of the applied voltage and any ME constant α

It must be noted that the profile of R_{pp} in Fig. 3a does not actually depend on the value of the ME constant α, and this is also true of the dependency of the other diagonal reflectivity R_{ss} (see solid blue line in Fig. 4). Its modulus $|R_{ss}|$ is of the same order of magnitude as that of R_{pp}, but is independent from the applied voltage, since its variation is directly related to that of permittivity tensor element $\varepsilon_{yy}^{(LC)}$ in the LC, which does not depend on the voltage-imposed tilt angle ϕ [see Fig. 3]. In contrast, the off-diagonal components $R_{ps}=R_{sp}$ do depend in a noticeable way on the ME coupling in the YIG layer, as can be seen from the comparison between Fig. 3b, where that coupling is neglected ($\alpha=0$), and Fig. 3c, where it is accounted for ($\alpha=\alpha^{(\mathrm{YIG})}$).

The most visible changes in the reflection coefficients take place, for any incidence angle, at near-threshold values of the applied voltage, as shown in the insets to Fig. 3. As one can see from Fig. 2, the tilt angle experiences an abrupt increase in the 1.0–1.3 V voltage range, which strongly modifies the reflection coefficients. Even a very small increase of the voltage above V_{th} results in a dramatic shift of the extrema of all reflection coefficients towards lower values of θ. The inset in Fig. 3a shows that, for instance, the angular position of a first minimum of $|R_{pp}|$ shifts from $\theta\approx35°$ at any voltage below V_{th} to $\theta=0°$ at $V\approx1.02$ V, and a second minimum, initially found at grazing incidence, shifts to normal incidence at $V\approx1.08$ V. Similarly, the local maximum of $|R_{pp}|$ initially found at $\theta\approx55°$ rapidly shifts towards lower values of θ above V_{th}, with an additional increase of its magnitude from 0.6 (at $V<V_{\mathrm{th}}$) to 0.8 (at $V\approx1.04$ V). Such rapid changes can be attributed to the strong increase of the tilt angle of the LC molecules in most of the cell thickness, i.e., away from its boundaries, where anchoring acts against molecular rotation (see Fig. 2), and the corresponding variation of the LC permittivity tensor elements. As one can expect from Fig. 2, a further increase of the applied voltage above approximately 2 V does not dramatically increase the value of the reflection coefficients, since the tilt angle then reaches a saturation value in most of the LC cell thickness.

Thus, the applied voltage allows to control the value of the diagonal reflection coefficient R_{pp} which can be attributed to the presence in the system of the inhomogeneous uniaxial LC cell. Indeed, such a control was found to be impossible in a similar structure where the electro-optic layer consisted of a homogeneous cubic ZnSe film, in which case only the off-diagonal reflection coefficients could be modified by an externally applied electric field/voltage [13].

The influence of the ME interaction on the off-diagonal reflection coefficient $R_{ps}=R_{sp}$ is made clear by comparing Fig. 3b and c. When the ME coupling is neglected ($\alpha=0$, Fig. 3b), the overall dependence of $|R_{ps}|$ upon the applied voltage is roughly similar to that of $|R_{pp}|$ (see Fig. 3a). When, on the other hand, it is accounted for ($\alpha=\alpha^{(\mathrm{YIG})}$, Fig. 3c), the behavior of $|R_{ps}|$ is strikingly different, with

the formation of a second maximum around $\theta \approx 40°$ below threshold voltage V_{th}, and a noticeable narrowing of the angular range over which the applied voltage influences the off-diagonal reflection coefficient of the system above V_{th} ($20° < \theta < 70°$ instead of the entire range of incidence angle). The values of $|R_{ps}|$ in this region are one order of magnitude larger than when the ME coupling is negligible ($\alpha = 0$). Outside this interval, towards normal or grazing incidence, the values of $|R_{ps}|$ are similar with or without ME interaction. It should be noted that the amplitude of the off-diagonal reflection coefficient $R_{ps} = R_{sp}$ is, in any case, two to three orders of magnitude smaller than those of the diagonal reflection coefficients R_{pp} and R_{ss}.

3.2 Goos–Hänchen shift

As mentioned earlier, and in accordance with Eq. (8), the different components of the reflection matrix, and thus the values of the GHS obtained for any combination of incident and reflected states of polarization can be separately evaluated. Practically, this simply requires the use of a polarizer and an analyzer placed on the path of the incoming and reflected beams, respectively.

Like the reflection coefficient R_{ss}, the corresponding GHS ΔX_{ss} is independent from both the applied voltage and the ME constant. It varies, however, with the angle of incidence of the light beam (dashed red line in Fig. 4), and its value remains positive for all θ, and varies between 0 at normal incidence and $+3.5\lambda_0$ at grazing incidence.

As with reflection coefficients, the behavior of the three other GHSs is complex, as it also depends on the voltage applied to the LC cell and on the value of the ME constant in the YIG film. Figure 5 shows the dependences of the reduced diagonal GHS ΔX_{pp} (Fig. 5a) and the off-diagonal GHS $\Delta X_{sp} = \Delta X_{ps}$ (Fig. 5b for $\alpha = 0$ and 5c for $\alpha = \alpha^{(YIG)}$) upon the incidence angle θ of the light beam and the applied voltage. Symbols in the insets correspond to some of the local maxima of the shift and thus coincide with identical symbols in the insets of Fig. 3, at angular positions and applied voltages where the reflection coefficients exhibit fast variations. As follows from (7), the variations of the GHS can be related to those of the reflection coefficients. In particular, rapid changes (with respect to the incidence angle, hence to $k_x = |\boldsymbol{k}| \sin\theta$) of the modulus and/or the phase of a reflection coefficient yield large values of the corresponding GHS in the same angular vicinity (compare for instance identical symbols in the insets of Figs. 3a, 5a). Note that the second term in (7) becomes negligible for large values of the beam waist w_0, in which case the expression of the GHS reduces to that first derived by Artmann [2].

It can be noted that the largest values of the diagonal GHS ΔX_{pp} coincide with relatively large values of the corresponding reflection coefficient R_{pp}. This is strikingly different from what was recently reported about similar multilayered systems [13, 27], in which large values of the beam shift coincided with minima of reflectivity. Even lower values of the GHS can be obtained for relatively large reflectivities. For example, for $V < V_{th}$, a positive maximum of ΔX_{pp} of about $+15\lambda_0$ appears around $\theta \approx 34°$ and corresponds to $|R_{pp}| \approx 0.2$ (see Figs. 3a, 5a). Increasing the voltage above threshold at the same incidence angle allows to significantly reduce the value of the GHS down to approximately $+8\lambda_0$ while keeping high values of $|R_{pp}|$ up to 0.8. Moreover, at large incidence angles ($\theta > 70°$), the application of the voltage can induce sign reversals of the GHS which varies in this region between $+20\lambda_0$ and $-30\lambda_0$, again with significant values of the reflectivity. These sign reversals can be attributed in particular to voltage-dependent changes of the permittivity tensor elements of the LC and thus to varying

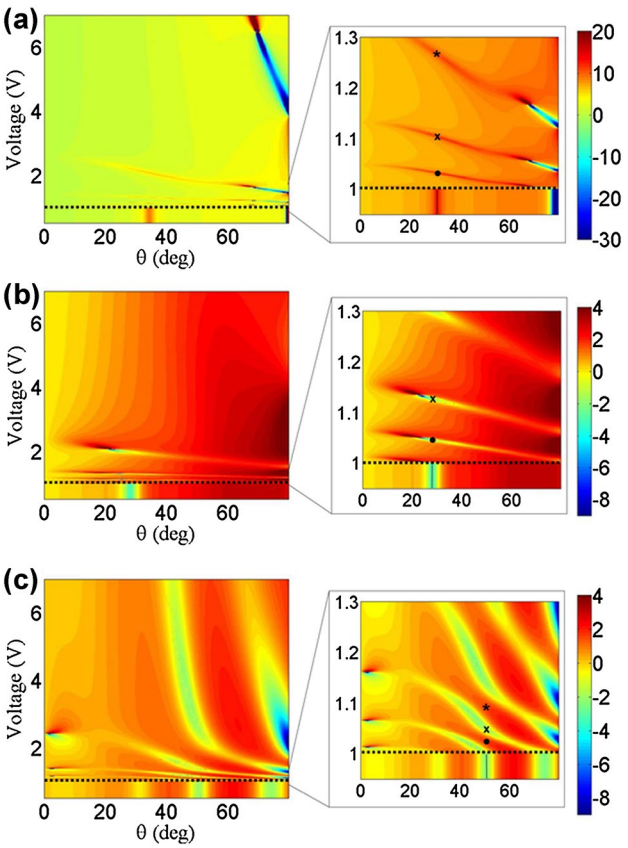

Fig. 5 Evolution of the GHS with incidence angle θ and applied voltage: **a** ΔX_{pp} for any value of the ME constant α; **b** ΔX_{ps} for $\alpha = 0$; **c** ΔX_{ps} for $\alpha = \alpha^{(YIG)}$. Insets show the corresponding GHS for near-threshold values of the applied voltage. The *black dotted lines* denote the threshold voltage $V_{th} = 1$ V. *Symbols* (•, ×, *) denote points of comparison between GHS in this figure and reflection coefficients in Fig. 3

conditions for constructive and destructive interference between the waves propagating in the system.

In contrast to the diagonal GHS, the off-diagonal ΔX_{ps} does not exceed a few λ_0, whether the ME interaction in YIG can be neglected (Fig. 5b) or not (Fig. 5c). Unlike ΔX_{pp}, however, it can exhibit sign reversal over large domains of θ when the applied voltage increases. For instance, in the case of a strong ME coupling in the YIG layer, ΔX_{ps} can change from a negative maximum of about $-2.5\lambda_0$ around $\theta \approx 55°$ in the sub-threshold regime ($V < V_{\text{th}}$) to a positive maximum of about $+2\lambda_0$ above threshold voltage (see symbols • and * in the inset of Fig. 5c). In this case, maximal positive values of ΔX_{ps} correspond to maximal values of $|R_{ps}|$ (compare • and * in the insets of Figs. 3c, 5c) and maximal negative values of ΔX_{ps} coincide with local minima of $|R_{ps}|$ [compare × in the insets of Figs. 3c, 5c]. A similar behavior can be observed over a broad range of incidence angles. In comparison, for a negligibly small ME coupling in the YIG layer, such a GHS sign reversal is only possible around $\theta \approx 25°$ [see symbols • and × in insets of Figs. 3b, 5b].

Apart from an externally applied voltage, another possibility to alter the GHS is via the application of an external magnetic field to reverse the saturation magnetization in the YIG layer towards negative values of z. Our calculations show that, while such a reversal almost does not affect the diagonal GHSs ΔX_{pp} and ΔX_{ss}, it does lead to a reversal of the sign of ΔX_{ps}, but only in some limited intervals of incidence angle and voltage. This stands in contrast to the behavior of a similar heterostructure, where a ZnSe film acted as an electro-optic layer, and in which a non-reciprocal sign change of the off-diagonal GHS could be obtained in all ranges of incidence angle θ and externally applied electric field [13]. Such a difference in behavior can be attributed mostly to the more intricate variations of the permittivity in the inhomogeneous LC cell than in the homogeneous ZnSe film, which, along with the interplay between magneto-optic and ME coefficients, affect the dependences of the reflectivity coefficients. However, as detailed in Sect. 4, the absolute value of ΔX_{ps} in this system can nevertheless, for well-chosen incidence angle and applied voltage, be enhanced by up to two orders of magnitude upon magnetization reversal.

In conclusion, our calculations show that the voltage-dependent reflection matrix components R_{pp} and $R_{sp} = R_{ps}$ have a significantly greater effect on the Goos–Hänchen shift than voltage-independent reflection coefficient R_{ss}.

4 Scheme for a gas sensor

As mentioned in the introduction, there have been numerous attempts at suggesting and implementing various sensors whose operation is based on the detection of an optical beam shift triggered by modifications of the local environment of the device (pressure, temperature, etc.). Here, we propose the principle of a gas sensor exploiting small but measurable variations of the dielectric constant of air. Calculations above were carried out assuming that the medium from which the incident light beam comes is vacuum or, indeed, air, i.e., for an upper medium permittivity equal to vacuum permittivity ε_0. In the presence of vapors, the relative permittivity of air has been shown to exhibit an absolute change of the order of a few 10^{-4} [5, 7] that is large enough to induce detectable variations of the longitudinal shift of an incoming light beam upon reflection from the multilayered structure studied in this paper.

Figure 6 illustrates the potential sensitivity of GHS measurements as a tool for detecting slight changes in the relative permittivity of air $\varepsilon^{(\text{air})}$ due to the presence of chemical vapors. The variation of the reduced diagonal GHS ΔX_{pp} is presented as a function of the near-threshold applied voltage for two values of $\varepsilon^{(\text{air})}$ for an angle of incidence of light of 70°. This variation is only measurable when ΔX_{pp} reaches its negative maximum around $V = 1.008$ V. As shown in the right inset of Fig. 6, the difference between the maximum values of the GHS for $\varepsilon^{(\text{air})} = 1$ (pure air, solid black line) and $\varepsilon^{(\text{air})} = 1.0005$ (air mixed with a chemical vapor, dotted red line) reaches up to $9\lambda_0$ (from about $-123\lambda_0$ for $\varepsilon^{(\text{air})} = 1$ to $-132\lambda_0$ for $\varepsilon^{(\text{air})} = 1.0005$), which makes it easily measurable in the near infra-red regime. The left inset of the figure shows that this difference (an increase in absolute value) is almost linear with the variation of $\varepsilon^{(\text{air})}$. The sensitivity of such a technique can be defined as

$$S = \frac{d(\Delta L_{\max})}{d\varepsilon^{(\text{air})}}, \tag{9}$$

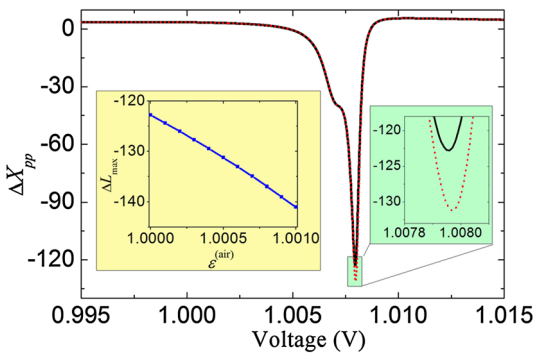

Fig. 6 Reduced GHS ΔX_{pp} vs applied voltage for two values of the relative dielectric permittivity of air: $\varepsilon^{(\text{air})} = 1$ (*solid black line*) and $\varepsilon^{(\text{air})} = 1.0005$ (*dotted red line*). Here, $d_{\text{LC}} = 3$ μm, $\theta = 70°$, and $w_0 = 30$ μm. The *right inset* zooms on the region where ΔX_{pp} reaches its negative peak value. The *left inset* shows the quasi-linear change of that peak value when $\varepsilon^{(\text{air})}$ varies from 1 to 1.0005

where $\Delta L_{\max}$ is the absolute value of the measured GHS peak amplitude. The average sensitivity in the conditions of Fig. 6 is 1.8×10^4 μm per unit of relative permittivity.

A similar impact of a change of the permittivity of air can be observed for the off-diagonal GHS. However, the direction of saturation magnetization **M** in the YIG film strongly influences the sensitivity of the technique. Figure 7 shows the variation of the reduced off-diagonal GHS ΔX_{ps} as a function of applied voltage in the same multilayer, and for the same two values of $\varepsilon^{(\text{air})}$ and the same angle of incidence of the incoming light beam as in Fig. 6. As seen previously, however, the ME interaction plays an important part in the variation of ΔX_{ps} (here, the ME constant is taken equal to $\alpha^{\alpha(\text{YIG})}$). The GHS remains at least two orders of magnitude smaller for $\mathbf{M} = +M_s\hat{z}$ (dashed blue line) than for $\mathbf{M} = -M_s\hat{z}$, where it reaches a large positive peak value (about $70\lambda_0$) around $V = 1.273$ V.

Moreover, while the beam shift is almost insensitive to a change of $\varepsilon^{(\text{air})}$ for $\mathbf{M} = +M_s\hat{z}$, it experiences a decrease of about 0.6 λ_0 for $\mathbf{M} = -M_s\hat{z}$ when $\varepsilon^{(\text{air})}$ varies from 1 (pure air, solid black line) to $\varepsilon^{(\text{air})} = 1.0005$ (air mixed with a chemical vapor, dotted red line). Although measurable, such a variation remains less pronounced than that observed with the diagonal GHS ΔX_{pp}. Accordingly, the sensitivity of the technique when ΔX_{ps} is considered is 1.6×10^3 μm per unit of relative permittivity, one order of magnitude smaller than that obtained for ΔX_{pp}. However, the sensitivity of the technique using the measurement of ΔX_{ps} could be greatly enhanced in a system including several ME layers, for instance if the LC cell capped a multilayered photonic crystal consisting of repeated YIG-GGG bilayers.

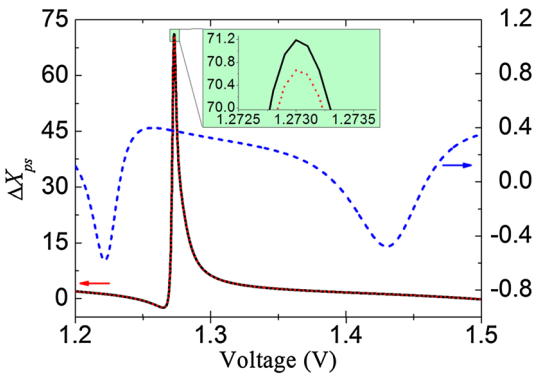

Fig. 7 Reduced GHS ΔX_{ps} vs applied voltage for two values of the relative dielectric permittivity of air: $\varepsilon^{(\text{air})} = 1$ (*solid black line*) and $\varepsilon^{(\text{air})} = 1.0005$ (*dotted red line*) when magnetization $\mathbf{M} = -M_s\hat{z}$. The *dashed blue line* shows ΔX_{ps} for $\mathbf{M} = +M_s\hat{z}$. Here, $d_{\text{LC}} = 3$ μm, $\theta = 70°$, and $w_0 = 30$ μm. The inset shows the voltage domain for which the GHS reaches its positive peak value in the former case

5 Conclusions

We have investigated the longitudinal Goos–Hänchen effect in a multilayered heterostructure consisting of a nematic liquid-crystal cell sandwiched between transparent electrodes and deposited on a magneto-electric/non-magnetic bilayer. The polarization-dependent variations of the Goos–Hänchen shift experienced by an optical beam upon reflection on the upper surface of the system have been studied as functions of both the dc electric voltage applied to the cell and the direction of the magnetization in the magnetic layer.

Our calculations show that the Goos–Hänchen shift of the reflected beam can be efficiently tuned via the external voltage applied to the liquid-crystal cell to modify the collective orientation of the molecules and thus their dielectric permittivity tensor components. The spatial inhomogeneity of the liquid crystal due to anchoring of the molecules at the cell boundaries has been taken into account. Its impact on the reflectivity of the structure and the Goos–Hänchen shift of the reflected light beam has been demonstrated for applied voltages slightly higher than the threshold value above which liquid-crystal reorientation occurs. Moreover, the impact of a magnetization reversal in the magneto-electric layer on the shift has been shown to be noticeable, but only for the *p* (resp., *s*) component of the reflected beam produced by an *s*- (resp., *p*-) polarized incident beam, and only in limited domains of incidence angle and applied voltage.

The results obtained with the Goos–Hänchen shift have led us to propose a scheme for a vapor detection technique using the variations of the shift due to changes of relative permittivity in the air surrounding the system. For well-chosen values of the applied voltage, even tiny vapor-induced variations of that permittivity can lead to shifts of the order of several hundreds of wavelengths for *p*-polarized reflected light produced by a *p*-polarized incident beam. The estimated sensitivity of such a technique is 1.8×10^4 μm per unit of relative permittivity. On the other hand, the Goos–Hänchen shift of *p*-polarized reflected light produced by *s*-polarized incident light (and vice versa) can be enhanced up to several tens of wavelengths by controlling the magnetization direction of the magneto-electric film. In this case, the sensitivity of the technique is about 1.6×10^3 μm per unit of relative permittivity.

Acknowledgements This work is supported in part by the Russian Science Foundation (Project 15-19-10036), the Ministry of Education and Science of the Russian Federation (Project 14.Z50.31.0015 and State Contract No. 3.7614.2017/П220), and by École Nationale d'Ingénieurs de Brest (Grant 14MOESMOMO14).

References

1. F. Goos, H. Hänchen, Ann. Phys. **436**, 333 (1947)
2. K. Artmann, Ann. Phys. **437**, 87 (1948)
3. K.Y. Bliokh, A. Aiello, J. Opt. **15**, 14001 (2013)
4. X. Wang, C. Yin, Z. Cao, *Progress in planar optical waveguides* (Springer, Berlin, 2015), pp. 163–189
5. Y. Nie, Y. Li, Z. Wu, X. Wang, W. Yuan, M. Sang, Opt. Express **22**, 8943 (2014)
6. J. Sun, X. Wang, C. Yin, P. Xiao, H. Li, Z. Cao, J. Appl. Phys. **112**, 83104 (2012)
7. T. Tang, C. Li, L. Luo, Y. Zhang, J. Li, Appl. Phys. B **122**, 1 (2016).
8. Z. Tahmasebi, M. Amiri, Phys. Rev. A **93**, 4382 (2016)
9. T. Tang, L. Luo, W. Liu, X. He, Y. Zhang: Appl. Phys. B **120**, 497 (2015).
10. T. Tang, J. Qin, J. Xie, L. Deng, L. Bi, Opt. Express **22**, 27042 (2014)
11. R. Macêdo, R.L. Stamps, T. Dumelow, Opt. Express **22**, 28467 (2014)
12. C. Luo, X. Dai, Y. Xiang, S. Wen, IEEE Photonics J. **7**, 6100310 (2015)
13. Y.S. Dadoenkova, F.F.L. Bentivegna, N.N. Dadoenkova, R.V. Petrov, I.L. Lyubchanskii, M.I. Bichurin, J. Appl. Phys. **119**, 203101 (2016)
14. Y.S. Dadoenkova, F.F.L. Bentivegna, N.N. Dadoenkova, R.V. Petrov, I.L. Lyubchanskii, M. I. Bichurin, J. Phys. Conf. Ser. **741**, 12201 (2016)
15. H. Sattari, S. Ebadollahi-Bakhtevar, M. Sahrai, J. Appl. Phys. **120**, 133102 (2016)
16. X. Wang, C. Yin, J. Sun, J. Gao, M. Huang, Z. Cao, J. Opt. **15**, 14007 (2013)
17. T. Rasing, I. Muševič, *Surfaces and interfaces of liquid crystals* (Springer, Berlin, 2004)
18. S. Isaacs, F. Placido, I. Abdulhalim, Appl. Opt. **53**, H91 (2014)
19. N. Goswami, A. Kar, A. Saha, Opt. Commun. **330**, 169 (2014)
20. H. Wang, Z. Zhou, H. Tian, Y. Pei, J. Phys. D. Appl. Phys. **42**, 175301 (2009)
21. B.B. Krichevtsov, V.V. Pavlov, R.V. Pisarev, A.G. Selitsky, Ferroelectrics **161**, 65 (1993)
22. I. Abdulhalim, D. Menashe. Liq. Cryst. **37**, 233 (2010)
23. D.-K. Yang, S.-T. Wu, *Fundamentals of liquid crystal devices*. (Wiley, Hoboken, 2016)
24. T.H. O'Dell, *The Electrodynamics of magnetoelectric media*. (North-Holland, Amsterdam, 1970)
25. K. Zvezdin, V.A. Kotov, *Modern magnetooptics and magnetooptical materials*. (Institute of Physics Publishing, Bristol, 1997)
26. P. Yeh, *Optical waves in layered media*. (Wiley, New York, 1988)
27. Y.S. Dadoenkova, F.F.L. Bentivegna, N.N. Dadoenkova, I.L. Lyubchanskii, Y.P. Lee, J. Opt. Soc. Am. B **33**, 393 (2016)
28. M. Fiebig, J. Phys. D **38**, R123 (2005)
29. T.A.F. König, P.A. Ledin, J. Kerszulis, M.A. Mahmoud, M.A. El-Sayed, J.R. Reynolds, V.V. Tsukruk, ACS Nano **8**, 6182 (2014)
30. K.-H. Hellwege, A.M. Hellwege *Landolt-Börnstein-Group III, Condensed Matter, Vol. 12a, Magnetic and other properties of oxides and related compounds-Part A: Garnets and Perovskites* (Springer, Berlin, 1978)
31. M. Torfeh, H. Le Gall, Phys. Status Solidi A **63**, 247 (1981)